Zero-Sequence Current Suppression Strategy of Open-Winding PMSG System With Common DC Bus Based on Zero Vector Redistribution

Yijie Zhou and Heng Nian, *Member, IEEE*

***Abstract*—The open-winding configuration with a common dc bus provides a zero-sequence current loop which allows the zero-sequence current flowing. With the application in permanent magnet synchronous generator (PMSG) systems, the existing zero-sequence current is inevitably caused by the common mode voltage generated by pulsewidth modulation (PWM) techniques and the third back EMF by the inherent flux harmonic component. With the mathematical modeling analysis, the zero-sequence equivalent circuit based on the PMSG system is proposed. Meanwhile, a zero-sequence current suppression controller is designed. In this paper, a zero vector redistribution PWM technique is proposed. With this technique, the dwell times of zero vectors (000) and (111) for both converters are determined. Meanwhile, it gives the zero-sequence component overmodulation analysis. Both the control method and improved PWM technique are implemented in a 1-kW open-winding PMSG experimental setup, and the experimental results are discussed.**

***Index Terms*—Dwell time, open-winding permanent-magnet synchronous generator (PMSG) system, zero-sequence current suppression, zero vector redistribution (ZVR) pulsewidth modulation (PWM) technique.**

I. Introduction

THE permanent-magnet synchronous generator (PMSG) has been widely applied due to its high power density, flexible magnet topologies, and excellent operation performance [1]–[3]. Nowadays, it has been employed in various industry applications, such as wind power generation systems, distribution generation systems, portable generation unit, etc. In order to achieve the stable operation of PMSG, it is usual to adopt a back-to-back full power rating converter to implement the power generation from PMSG to the grid or local load.

Considering the stringent requirements on the converter in the large-power PMSG system, the open-winding configuration offers advantages over the traditional star or delta-connected PMSG. By applying two voltage-source converters (VSCs) to both ends of the stator windings, the open-winding PMSG system cannot only reduce the dc bus voltage by half but also achieve a multilevel modulation effect [4]–[6]. Generally, the open-winding systems can employ a common dc bus [7] or two isolated dc buses [8]. Compared with the two isolated dc buses, a common dc bus based open-winding system has a simple structure and an easy implementation for practical applications such as wind power generation, electric vehicle, etc. However, the common dc bus provides a zero-sequence current circuit for the open-winding PMSG, and the zero-sequence currents will flow through the stator windings, which will increase the system losses and decrease the operation efficiency [9]–[11]. Furthermore, because the third back electromotive force (EMF) usually exists in the phase windings of the PMSG [12], the zero-sequence current also will produce a six times frequency torque ripple.

To suppress the zero-sequence current on the common dc bus, a common mode voltage (CMV) elimination strategy for an induction motor drive was proposed in [13]. By combining a certain voltage vector to obtain the same CMV contribution on both converter sides, zero-sequence voltage (ZSV) for stator windings can be avoided. The works reported in [14] and [15] investigated the zero vector placement technique on the open-winding induction motor with decoupled space vector pulsewidth modulation (SVPWM) and subhexagonal center PWM switching scheme. It can be found that the zero vector time determines the CMV and zero-sequence current of induction motors. In summary, the zero-sequence current suppression implementation of the open-winding induction motor is focused on the elimination of CMV generated by the dual converters.

The rotor flux generated by a permanent magnet always contains the rich harmonic components, especially the third harmonic component, which usually behaves as the CMV. Therefore, the existing CMV elimination strategy in the open-winding induction motor is unavailable for the open-winding PMSG to suppress the zero-sequence current. An active CM compensator was proposed to reduce the third harmonic current in a half-controlled converter-based open-winding PMSG system in [16]. Reference [17] proposed a zero-axis current regulator to suppress the zero-sequence current for the open-winding PMSG. Both [16] and [17] achieved third current component suppression based on the sine-wave PWM. However, because the third back EMF component and CMV reference will change on different rotation speeds, the effect mechanism of the active voltage vectors and zero voltage vectors on the CMV is not analyzed. Considering that the active voltage vector is obtained according to the fundamental frequency voltage reference, the

Manuscript received May 15, 2014; revised August 5, 2014 and September 11, 2014; accepted October 12, 2014. Date of publication November 3, 2014; date of current version May 8, 2015.

The authors are with the College of Electrical Engineering, Zhejiang University, Hangzhou 310027, China (e-mail: zhouyijie@zju.edu.cn; nianheng@zju.edu.cn).

Color versions of one or more of the figures in this paper are available online at http://ieeexplore.ieee.org.

Digital Object Identifier 10.1109/TIE.2014.2366715

CMV regulation technique based on the dwell times of zero vectors is the key factor to suppress the zero-sequence current, which is also analyzed in this paper.

In order to eliminate the zero-sequence current, a circulating current elimination strategy of the open-winding PMSG system based on zero vector redistribution (ZVR) is proposed in this paper. First, the mathematical model of the open-winding PMSG with the consideration of third harmonic flux will be developed. Moreover, an overall control diagram of the open-winding PMSG system is proposed to suppress the zero-sequence current. The effect mechanism of the zero vectors on the CMV is analyzed, and the ZVR technique is proposed. Furthermore, the linear modulation range of the ZVR PWM is investigated. Finally, a 1-kW experimental setup is built to validate the availability of the proposed control method and modulation technique.

II. Zero-Sequence Circuit Modeling of Open-Winding PMSG

The back EMF of the open-winding PMSG usually contains the third harmonic component, which is different from the open-winding induction motor. In order to analyze and suppress the zero-sequence current in the open-winding PMSG system with the common dc bus, the mathematical model of the open-winding PMSG including the zero-axis equation should be developed.

The phase voltage equations of the open-winding PMSG can be expressed as [18]

$$\begin{bmatrix} u_a \\ u_b \\ u_c \end{bmatrix} = \frac{d}{dt}\begin{bmatrix} \psi_a \\ \psi_b \\ \psi_c \end{bmatrix} - \begin{bmatrix} R_a & & \\ & R_b & \\ & & R_c \end{bmatrix}\begin{bmatrix} i_a \\ i_b \\ i_c \end{bmatrix} \tag{1}$$

where u is the phase voltage, R is the phase resistance, i is the phase current, Ψ is the stator flux, and subscripts a, b, c represent the component of a, b, c phase, respectively.

Defining the fundamental and third harmonic component amplitudes of the rotor flux linkage as Ψ_r and Ψ_{3r}, the flux equation can be expressed as

$$\begin{bmatrix} \psi_a \\ \psi_b \\ \psi_c \end{bmatrix} = -\begin{bmatrix} L_S & M_S & M_S \\ M_S & L_S & M_S \\ M_S & M_S & L_S \end{bmatrix}\begin{bmatrix} i_a \\ i_b \\ i_c \end{bmatrix} + \begin{bmatrix} \psi_r \cos(\theta_r) + \psi_{3r}\cos(3\theta_r) \\ \psi_r \cos(\theta_r - \frac{2}{3}\pi) + \psi_{3r}\cos(3\theta_r) \\ \psi_r \cos(\theta_r + \frac{2}{3}\pi) + \psi_{3r}\cos(3\theta_r) \end{bmatrix} \tag{2}$$

where L_S and M_S represent the self-inductance and mutual inductance, separately, and θ_r is the rotor position angle.

When the d-axis is aligned at the direction of the rotor flux, based on the transformation matrix from the three-phase stationary abc coordinate frame to the synchronous rotating $dq0$ coordinate frame shown in (3), the flux linkage in the $dq0$ frame can be represented as (4)

$$T_{\frac{3S}{3R}} = \frac{2}{3}\begin{bmatrix} \cos(\theta_r) & \cos(\theta_r - 120^\circ) & \cos(\theta_r + 120^\circ) \\ -\sin(\theta_r) & -\sin(\theta_r - 120^\circ) & -\sin(\theta_r + 120^\circ) \\ \frac{1}{2} & \frac{1}{2} & \frac{1}{2} \end{bmatrix} \tag{3}$$

$$\begin{bmatrix} \psi_d \\ \psi_q \\ \psi_0 \end{bmatrix} = T_{\frac{3S}{3R}}\begin{bmatrix} \psi_a \\ \psi_b \\ \psi_c \end{bmatrix}$$

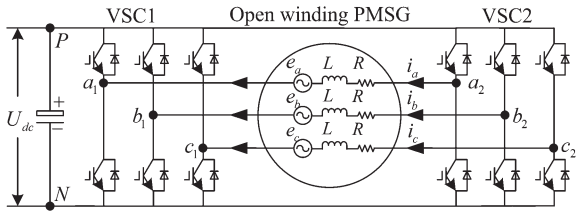

Fig. 1. Open-winding PMSG system with a common dc bus.

$$= -\begin{bmatrix} L_d & & \\ & L_q & \\ & & L_0 \end{bmatrix}\begin{bmatrix} i_d \\ i_q \\ i_0 \end{bmatrix} + \begin{bmatrix} \psi_r \\ 0 \\ \psi_{3r}\cos(3\theta_r) \end{bmatrix} \tag{4}$$

where the subscripts d, q, and 0 represent the components in $dq0$ frame, respectively.

Thus, the voltage equation in $dq0$ frame can be written as

$$\begin{bmatrix} u_d \\ u_q \\ u_0 \end{bmatrix} = \begin{bmatrix} -L_d\frac{di_d}{dt} - Ri_d + \omega L_q i_q \\ -L_q\frac{di_q}{dt} - Ri_q - \omega L_d i_d + \omega\psi_r \\ -L_0\frac{di_0}{dt} - 3\omega\psi_{3r}\sin(3\theta_r) - Ri_0 \end{bmatrix}. \tag{5}$$

The electromagnetic torque can be expressed as

$$T_e = \frac{3}{2}n_p\left[L_q i_q i_d + (\psi_r - L_d i_d)i_q - 6\psi_{3r}\sin(3\theta_r)i_0\right]. \tag{6}$$

It can be seen that, when the zero-sequence current exists in the open-winding PMSG, six time frequency fluctuations in electromagnetic torque will occur, which is harmful to the steady operation of PMSG and deteriorates the lifetime of mechanical units. Thus, it is necessary to suppress the zero-sequence current in the open-winding PMSG system.

III. Suppression Strategy of Zero-Sequence Current

The open-winding PMSG system with common dc bus is shown in Fig. 1. Two VSCs VSC1 and VSC2 supplied by a common dc bus are connected to the stator winding. Based on the switch state of the semiconductor device, the instantaneous phase voltage model of the open-winding PMSG modulated by VSCs can be written as

$$\begin{cases} u_a = S_{a1}U_{\rm dc} - S_{a2}U_{\rm dc} \\ u_b = S_{b1}U_{\rm dc} - S_{b2}U_{\rm dc} \\ u_c = S_{c1}U_{\rm dc} - S_{c2}U_{\rm dc} \end{cases} \tag{7}$$

where S is the switching state of each bridge of the VSC, while $S = 1$ means that the switch device on the upper bridge arm turns on, and $S = 0$ means that the switch device on the lower bridge arm turns on; $U_{\rm dc}$ represents the dc-link voltage; subscripts a, b, and c represent the components of a, b, and c phases, respectively; and subscripts 1 and 2 represent the components of VSC1 and VSC2, respectively.

It can be seen from (7) that the phase voltage of the open-winding PMSG could be modulated as $U_{\rm dc}$, 0, $-U_{\rm dc}$ with different switch state combinations. Therefore, the open-end-winding configuration fed by two two-level inverters will still result in a three-level structure when driven by a single bus.

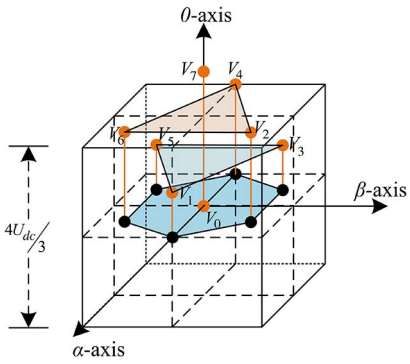

Fig. 2. Space vector modulation perspective in $\alpha\beta0$ 3-D frame.

TABLE I
VOLTAGE VECTOR DISTRIBUTION

	Vector	Switch state	Value	CMV
Zero vectors	V_0	(000)	0	0
	V_7	(111)	0	U_{dc}
Active vectors	V_1	(100)	$2U_{dc}/3$	$U_{dc}/3$
	V_2	(110)	$U_{dc}/3+j\sqrt{3}\,U_{dc}/3$	$2U_{dc}/3$
	V_3	(010)	$-U_{dc}/3+j\sqrt{3}\,U_{dc}/3$	$U_{dc}/3$
	V_4	(011)	$-2U_{dc}/3$	$2U_{dc}/3$
	V_5	(001)	$-U_{dc}/3-j\sqrt{3}\,U_{dc}/3$	$U_{dc}/3$
	V_6	(101)	$U_{dc}/3-j\sqrt{3}\,U_{dc}/3$	$2U_{dc}/3$

In the two-phase stationary $\alpha\beta0$ coordinate frame, the phase voltage can be expressed as

$$\begin{bmatrix} u_\alpha \\ u_\beta \\ u_0 \end{bmatrix} = \begin{bmatrix} \frac{2}{3}S_{a1} - \frac{1}{3}S_{b1} - \frac{1}{3}S_{c1} \\ \frac{\sqrt{3}}{3}(S_{b1} - S_{c1}) \\ \frac{1}{3}S_{a1} + \frac{1}{3}S_{b1} + \frac{1}{3}S_{c1} \end{bmatrix} U_{\rm dc} - \begin{bmatrix} \frac{2}{3}S_{a2} - \frac{1}{3}S_{b2} - \frac{1}{3}S_{c2} \\ \frac{\sqrt{3}}{3}(S_{b2} - S_{c2}) \\ \frac{1}{3}S_{a2} + \frac{1}{3}S_{b2} + \frac{1}{3}S_{c2} \end{bmatrix} U_{\rm dc}. \quad (8)$$

Equation (8) could be rewritten as

$$u_{\alpha\beta0} = u_{\alpha\beta0\_1} - u_{\alpha\beta0\_2} \quad (9)$$

where $u_{\alpha\beta0}$ represents the stator voltage vector in $\alpha\beta0$ frame and $u_{\alpha\beta0-1}$ and $u_{\alpha\beta0-2}$ are the voltage vectors generated by VSC1 and VSC2, respectively.

In order to clarify the component of each voltage vector in $\alpha\beta0$ 3-D frame, according to (8) and (9), the voltage space vector modulation perspective of $V_{\alpha\beta0-1}$ and $V_{\alpha\beta0-2}$ in $\alpha\beta0$ frame is shown in Fig. 2. The side length of the cube linked by a solid line is $4U_{\rm dc}/3$. Eight yellow points represent eight different space vector locations as the switch state combination S_a, S_b, and S_c is 0 or 1. The projection on the $\alpha\beta$ plane is the same as the traditional hexagon structure in conventional vector diagram. Table I shows the voltage vector distribution, in which the amplitude value and zero-sequence component of each voltage vector are presented. It can be seen that the zero-sequence component can be calculated as $(S_a + S_b + S_c)U_{\rm dc}/3$ and has four statuses shown in Table I: 1) 0, for $V_0(000)$; 2) $U_{\rm dc}/3$, for $V_1(100)$, $V_3(010)$, and $V_5(001)$; 3) $2U_{\rm dc}/3$, for $V_2(110)$, $V_4(011)$, and $V_6(101)$; and 4) $U_{\rm dc}$, for $V_7(111)$. Thus, it can be concluded that the ZSV can be modulated by VSC1 and VSC2.

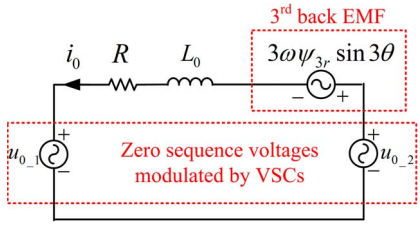

Fig. 3. Zero-sequence equivalent circuit of the open-winding PMSG system.

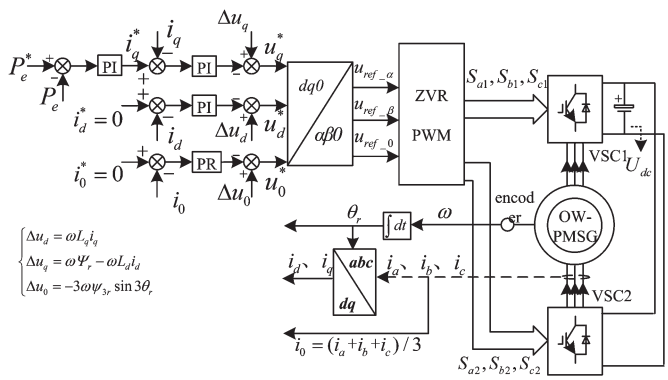

Fig. 4. Control scheme of the open-winding PMSG system with zero-sequence current suppression.

In the zero-sequence circuit of the open-winding PMSG system [16], ignoring the effect of the voltage drop and dead time on the switch device, the zero-sequence circulating current is generated mainly due to these two major causes:

1) the CMV generated by PWM;
2) the third harmonic component in back EMF.

According to the aforementioned analysis, the zero-sequence equivalent circuit of the open-winding PMSG system could be obtained as shown in Fig. 3, in which u_{0-1} and u_{0-2} are generated by VSC1 and VSC2, respectively, and $3\omega\Psi_{3r}\sin 3\theta$ is generated by the third back EMF. Thus, in order to suppress the zero-sequence current, the ZSV reference should be modulated to counteract the third harmonic component in back EMF.

The proposed control scheme of the zero-sequence current suppression for the open-winding PMSG system is shown as Fig. 4, in which a closed-loop regulator of the zero-sequence current is designed. The zero-sequence current i_0 could be calculated as one third of the sum of i_a, i_b, and i_c. Since the zero-sequence current is mainly a triple frequency ac component, a PR controller is selected to eliminate the tracking error [19]. Compared with [16], using the PR controller, zero-sequence current suppression is easy to implement. The common mode current regulator proposed in [16] is comparatively complex, which needs a third harmonic PLL and a PI regulator. The zero-sequence current reference i_0^* is set as 0, and a PR controller with the resonant frequency tuned at the third fundamental frequency is used as a zero-sequence current regulator to obtain the ZSV reference. According to (5), a compensation

$-3\omega\Psi_{3r}\sin 3\theta_r$ is adopted for the zero-sequence current suppression regulator. Therefore, the ZSV reference can be calculated as

$$u_0^* = \left(k_P + \frac{k_R\omega_c s}{s^2+2\omega_c s+\omega_0^2}\right)(i_0^* - i_0) - 3\omega\psi_{3r}\sin 3\theta_r \quad (10)$$

where k_p and k_R represent the proportional and resonant gains of the zero-sequence current suppression regulator. ω_c is the cut-off frequency, while ω_0 is the resonant frequency. In order to implement zero-sequence current suppression, ω_0 is selected as 3ω, and ω_c can be selected as $2-5$ rad/s [20].

Similarly, the PI controllers for i_d and i_q are used to achieve d-axis and q-axis voltage references. The outer loop controller is designed to implement the power regulation for the generation system, and the output is set as the q-axis current reference value. Meanwhile, the rotor flux orientation control strategy is adopted for the open-winding PMSG. The ZVR PWM is employed to modulate the voltage reference, which will be introduced in Section IV. Thus, zero-sequence current suppression is implemented by both the closed-loop regulator of the zero-sequence current and ZVR PWM. By obtaining the ZSV reference, the proposed ZVR PWM technique could generate a required ZSV by redistributing the zero vector dwell time of two converters. The volt-second equivalent principle is still adopted in $\alpha\beta 0$ component modulation.

IV. PWM Technique Based On ZVR

The conventional SVPWM [21], [22] is usually employed to modulate the $\alpha\beta$ voltage reference. In general, the dwell times for two zero vectors (000) and (111) are equally divided. As for the open-winding PMSG system, the zero-sequence reference voltage will be modulated to suppress the zero-sequence current. Thus, the zero vector dwell time will be redistributed in two VSCs to satisfy the requirement of the ZSV reference. The principle of the zero vector dwell time redistribution is the volt-second equivalent principle, which is similar to the principle proposed in [14] and [15]. The volt-second equivalent principle is the foundation for almost all PWM techniques. Different from the analysis on zero vector placement in induction motors in [14] and [15], the redistribution concept in this paper is used to counteract the third back EMF in the open-winding PMSG and prepares for a further discussion on the ZSV modulation range.

The vector diagram of the $\alpha\beta$ plane on the combination of dual converters is shown in Fig. 5, in which VSC1 modulates vectors V_0-V_7 and VSC2 modulates vectors $V_0'-V_7'$. For the decoupled PWM strategy, the voltage reference on $\alpha\beta$ plane $u_{\mathrm{ref}-\alpha\beta}$ could be divided into two voltage vectors with equal and opposite directions as $u_{\alpha\beta-1}$ and $u_{\alpha\beta-2}$. Thus, the modulation voltage vectors $u_{\alpha\beta 1}$ and $u_{\alpha\beta-2}$ for both converters can be expressed as

$$u_{\mathrm{ref\_}\alpha\beta} = u_{\alpha\beta\_1} - u_{\alpha\beta\_2} = (u_{\alpha\_1} + ju_{\beta\_1}) - (u_{\alpha\_2} + ju_{\beta\_2}) \quad (11)$$

where $u_{\alpha-1} = -u_{\alpha-2,u\beta-1} = u_{\beta-2}$.

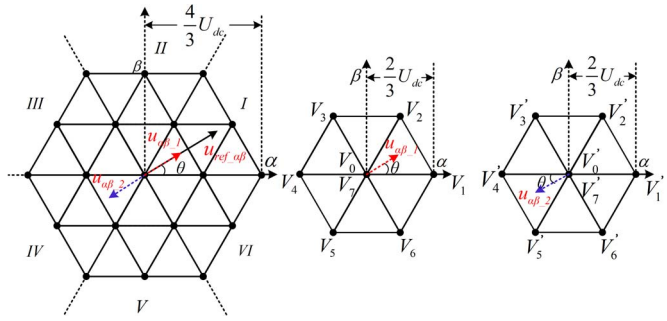

Fig. 5. Vector diagram of the $\alpha\beta$ plane on the combination of dual converters.

Taking $u_{\mathrm{ref\_}\alpha\beta}$ in region I as example, $u_{\alpha\beta-1}$ is in section I, while $u_{\alpha\beta-2}$ is in Section IV, as shown in Fig. 5. Thus, the dwell time for each vector can be calculated as

$$\begin{aligned}(u_{\alpha\_1} + ju_{\beta\_1})T_s &= V_0t_0 + V_1t_1 + V_2t_2 + V_7t_7\\ (u_{\alpha\_2} + ju_{\beta\_2})T_s &= V_0't_0' + V_5't_5' + V_4't_4' + V_7't_7'\\ T_s &= t_0 + t_1 + t_2 + t_7 = t_0' + t_5' + t_4' + t_7' \end{aligned} \quad (12)$$

where t_0, t_1, t_2, and t_7 represent the dwell times of vectors $V_0(000)$, $V_1(100)$, $V_2(110)$, and $V_7(111)$, respectively, while t_0', t_4', t_5', and t_7' represent the dwell times of vectors $V_0'(000)$, $V_4'(011)$, $V_5'(001)$, and $V_7'(111)$, respectively; T_s is the switching period.

Since $u_{\alpha\beta-1}$ and $u_{\alpha\beta-2}$ are equal in amplitude and opposite in direction, the effects of V_2 on $u_{\alpha\beta-1}$ and V_5' on $u_{\alpha\beta-2}$ are equivalent due to the vector symmetry. Therefore, it comes to that $t_2 = t_5'$. Moreover, the same conclusion that t_1 is equal to t_4' can be drawn with the same reason. Defining the modulation index $m = |u_{\mathrm{ref}-\alpha\beta}|/((2\sqrt{3}/3)U_{\mathrm{dc}})$, the dwell times of the active voltage vector can be deduced as [17]

$$t_1 = t_4' = \frac{\sqrt{3}m\sin(60^\circ-\theta)}{2\sin(60^\circ)}T_s,\ t_2 = t_5' = \frac{\sqrt{3}m\sin(\theta)}{2\sin(60^\circ)}T_s \quad (13)$$

where θ is the angle between $u_{\mathrm{ref}-\alpha\beta}$ and α-axis shown in Fig. 5.

In order to modulate the zero-axis voltage reference $u_{\mathrm{ref}-0}$, the zero vector dwell time should be redistributed. It should be noted that the active vector also can cause the ZSV. Moreover, the dwell time for the active vector has been determined by (13). According to the volt-second equivalent principle, the zero vector dwell time needs to be obtained to modulate $u_{\mathrm{ref}-0}$. As a result, the ZSV modulated by VSC1 and VSC2 can be expressed as (14.a) and (14.b). Hence, the relationship for the dwell times for t_7 and t_7' can be inferred as (14.c)

$$u_{0\_1}T_s = \frac{U_{\mathrm{dc}}}{3}t_1 + \frac{2U_{\mathrm{dc}}}{3}t_2 + U_{\mathrm{dc}}t_7 \quad (14.a)$$

$$u_{0\_2}T_s = \frac{2U_{\mathrm{dc}}}{3}t_4' + \frac{U_{\mathrm{dc}}}{3}t_5' + U_{\mathrm{dc}}t_7' \quad (14.b)$$

$$u_{\mathrm{ref\_}0}T_s = (u_{0\_1} - u_{0\_2})T_s = \frac{U_{\mathrm{dc}}}{3}t_2 - \frac{U_{\mathrm{dc}}}{3}t_1 + U_{\mathrm{dc}}(t_7 - t_7'). \quad (14.c)$$

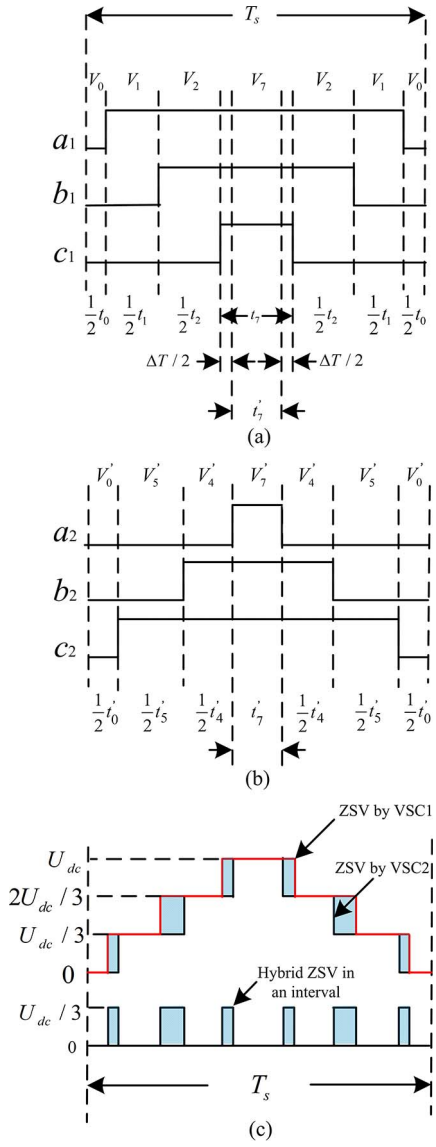

Fig. 6. Zero voltage vector redistribution scheme. (a) Modulation scheme for VSC1. (b) Modulation scheme for VSC2. (c) Hybrid ZSV modulated by VSC1 and VSC2.

According to (14.c), the deviation of zero vector (111) dwell time for both VSCs should be kept as $\triangle T$ to obtain a desired ZSV. It can be expressed as

$$\Delta T = t_7 - t_7' = \frac{u_{\text{ref\_0}}}{U_{\text{dc}}} T_s - \frac{1}{3}t_2 + \frac{1}{3}t_1 \tag{15}$$

where ΔT is defined as the ZVR time, which means the dwell time difference of voltage vector 111 between two converters.

Generally, in order to keep two VSCs operating on the symmetrical work state, the dwell times for zero vectors t_0, t_7, t_0', and t_7' can be redistributed and expressed as

$$\begin{aligned} t_7 = t_0' &= \frac{\Delta T}{2} + \frac{1}{2}(T_s - t_1 - t_2) \\ t_0 = t_7' &= -\frac{\Delta T}{2} + \frac{1}{2}(T_s - t_1 - t_2). \end{aligned} \tag{16}$$

Fig. 6(a) and (b) shows the zero voltage vector redistribution schemes within a switching period based on (12)–(16). The

TABLE II
DWELL TIMES OF VOLTAGE VECTORS

Section	t_L	t_H	ΔT
I	$-Z$	X	$u_{ref\_0}T_s/U_{dc}-(X+Z)/3$
II	Z	Y	$u_{ref\_0}T_s/U_{dc}+(Z-Y)/3$
III	X	$-Y$	$u_{ref\_0}T_s/U_{dc}+(X+Y)/3$
IV	$-X$	Z	$u_{ref\_0}T_s/U_{dc}-(X+Z)/3$
V	$-Y$	$-Z$	$u_{ref\_0}T_s/U_{dc}+(Z-Y)/3$
VI	Y	$-X$	$u_{ref\_0}T_s/U_{dc}+(X+Y)/3$

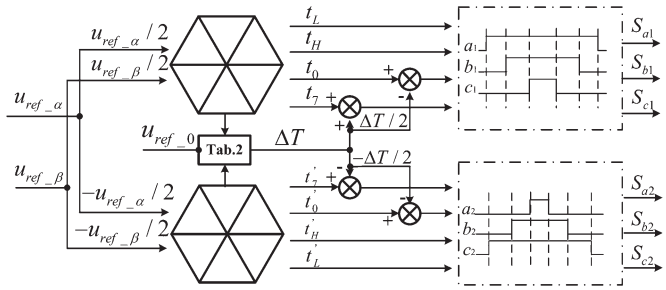

Fig. 7. PWM scheme based on zero voltage vector redistribution.

ZVR time $\triangle T$ is distributed equally and arranged in V_0 and V_7. The dwell times of each active vector could be determined based on the voltage reference $u_{\text{ref}-\alpha\beta 0}$. Thus, the zero vector dwell times of two converters can be represented as $t_0 + t_7$ and $t_0' + t_7'$, which is equal to $T_s - t_1 - t_2$. Moreover, the active time period can be kept unchanged within a switching period. In order to obtain the ZSV modulation process within an interval, Fig. 6(c) shows the ZSV modulated by both VSCs within an interval, and the hybrid ZSV is also presented to show the modulation process of the zero-sequence component.

Since the aforementioned analysis is based on the example that $u_{\text{ref}-\alpha\beta}$ is located in region I, the dwell times could be calculated with the same method as $u_{\text{ref}-\alpha\beta}$ in regions II–VI. The dwell time calculation of active vectors and $\triangle T$ for V_7 is given in (17) and Table II. In Table II, t_L represents the dwell times for active vectors which modulate the CMV as $U_{\text{dc}}/3$. On the other hand, t_H represents the dwell times for active vectors modulating the CMV as $2U_{\text{dc}}/3$. The dwell time calculation expression is named by X, Y, or Z. Therefore, it can be seen that the dwell time could be obtained by the look-up table as shown in Table II. Fig. 7 shows the implementation method of the PWM scheme based on zero voltage vector redistribution

$$\begin{cases} X = m\sin\theta T_s \\ Y = \frac{\sqrt{3}m\cos\theta + m\sin\theta}{2} T_s \\ Z = \frac{-\sqrt{3}m\cos\theta + m\sin\theta}{2} T_s. \end{cases} \tag{17}$$

Thus, as discussed previously, since the zero-sequence circuit exists in the open-winding system supplied by the single dc bus, it is necessary to control the ZSV as desired. Furthermore, the real-time CMV generated by both VSCs could be calculated according to the switching state as $(S_{a1} + S_{b1} + S_{c1} - S_{a2} - S_{b2} - S_{c2})U_{\text{dc}}/3$. It can be also regarded as the real-time ZSV component caused by the PWM technique, which means that all active vectors and zero vectors make contribution to the zero-sequence component. Therefore, in order to suppress the

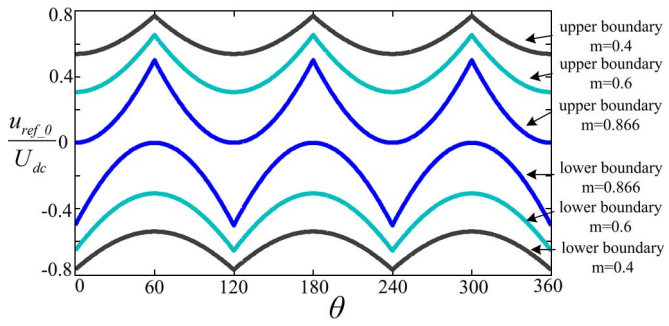

Fig. 8. Modulation boundary analysis of ZSV.

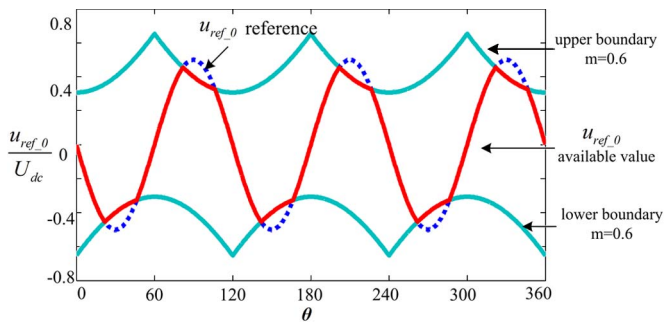

Fig. 9. Overmodulation for ZSV.

zero-sequence current, the zero vector dwell time should be redistributed to modulate the ZSV reference.

V. Available Modulation Range Analysis

For the ZVR PWM technique, the dwell times for active vectors and zero vectors are determined according to $u_{\mathrm{ref}-\alpha\beta 0}$. Therefore, when the switching period and voltage reference $u_{\mathrm{ref}-\alpha\beta}$ are fixed, the available modulation range for the ZSV reference is limited. The zero-sequence current could not be completely suppressed if the ZSV reference is beyond the available modulation range.

According to (14), the available modulation range of ZSV can be deduced as

$$\begin{aligned}&(u_{\mathrm{ref\_0}})_{\max}|\,(t_7'=0,t_7=T_s-t_1-t_2)\\&=\frac{1}{T_s}\left[\frac{U_{\mathrm{dc}}}{3}t_2-\frac{U_{\mathrm{dc}}}{3}t_1+U_{\mathrm{dc}}(T_s-t_1-t_2)\right]\\&=U_{\mathrm{dc}}\left[1-\frac{2\sqrt{3}}{3}m\cos\theta\right]\end{aligned}\tag{18}$$

$$\begin{aligned}&(u_{\mathrm{ref\_0}})_{\min}|\,(t_7=0,t_7'=T_s-t_4'-t_5')\\&=\frac{1}{T_s}\left[\frac{U_{\mathrm{dc}}}{3}t_2-\frac{U_{\mathrm{dc}}}{3}t_1-U_{\mathrm{dc}}\,(T_s-t_4'-t_5')\right]\\&=U_{\mathrm{dc}}\left[-1+\frac{2\sqrt{3}}{3}m\sin(30^\circ+\theta)\right].\end{aligned}\tag{19}$$

From (18) and (19), it can be found that the ZSV modulation range by VSCs is determined by the m value. By analyzing all six different regions, the relationship between ZSV and θ is shown in Fig. 8, in which the upper and lower boundaries with three different modulation indexes as $m=0.4$, $m=0.6$, and $m=0.866$ are given. When $\theta=60^\circ$, 180°, and 300°, the upper and lower boundaries can obtain the maximum and minimum values, respectively, in all modulation index ranges. In the opposite, when $\theta=0^\circ$, 120°, and 240°, the upper and lower boundaries can obtain the minimum and maximum values, respectively. It can be seen that the modulation region can cover a larger range if m decreases. In the case $m=0.866$, the maximum value of the upper boundary and the minimum value of the lower boundary are both zero.

The case study of overmodulation for ZSV is shown in Fig. 9, in which $m=0.6$. As $u_{\mathrm{ref}-0}$ is beyond the upper or lower boundary, the achievable ZSV cannot be modulated as expected. In this case, the available ZSV can just go along with the boundary until it returns back to the available modulation region as the red line trace.

Thus, the modulation index m determines the available maximum amplitude of $u_{\mathrm{ref}-0}$. The critical condition differentiating the available and overmodulation is that the ZSV reference trace is just intersected with the upper and lower boundaries. When the d-axis and zero-axis current is controlled as zero and the resistance is neglected, it can be inferred from (5) that the $dq0$-axis voltage on steady-state condition can be approximately expressed as

$$\begin{cases}u_d\approx\omega L_q i_q\\u_q\approx\omega\psi_r\\u_0\approx-E_3\sin(3\theta_r)\end{cases}\tag{20}$$

where $E_3=3\omega\Psi_{3r}$ is the amplitude of ZSV $u_{\mathrm{ref}-0}$.

When the ZSV reference is just intersected with the lower boundary, the relationship between the modulation index m and the maximum $u_{\mathrm{ref}-0}$ amplitude based on (18) and (19) can be described as

$$\begin{aligned}&U_{\mathrm{dc}}\left[-1+\frac{2\sqrt{3}}{3}m\sin(30^\circ+\theta_0)\right]=-E_{3\max}\sin(3\theta_0)\\&\frac{d}{dt}\left\{U_{\mathrm{dc}}\left[-1+\frac{2\sqrt{3}}{3}m\sin(30^\circ+\theta)\right]\right\}|_{\theta=\theta_0}\\&=\frac{d}{dt}\left\{-E_{3\max}\sin(3\theta_0)\right\}|_{\theta=\theta_0}\end{aligned}\tag{21}$$

where θ_0 is the horizontal ordinate value of the intersection point.

The maximum $u_{\mathrm{ref}-0}$ amplitude can be obtained when m is constant. Meanwhile, the $u_{\mathrm{ref}-0}$ amplitude is proportional to m in the open-winding PMSG system. Define k as the ratio between the amplitude of $u_{\mathrm{ref}-0}$ and $u_{\mathrm{ref}-\alpha\beta}$; thus, it can be expressed as

$$k=\frac{E_3}{|u_{\mathrm{ref}-\alpha\beta}|}=\frac{\sqrt{3}}{2}\frac{\frac{E_3}{U_{\mathrm{dc}}}}{\frac{|u_{\mathrm{ref}-\alpha\beta}|}{\frac{2\sqrt{3}}{3}U_{\mathrm{dc}}}}=\frac{\sqrt{3}}{2}\frac{\frac{E_3}{U_{\mathrm{dc}}}}{m}.\tag{22}$$

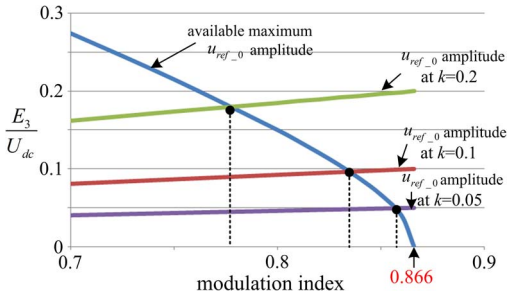

Fig. 10. Relationship between modulation index and $u_{\mathrm{ref}-0}$ amplitude.

According to (19), k can also be inferred as

$$k = \frac{E_3}{|u_{\mathrm{ref}-\alpha\beta}|} \approx \frac{3\psi_{3r}}{\sqrt{(\psi_r)^2 + (L_q i_q)^2}}. \tag{23}$$

Thus,

$$\frac{E_3}{U_{\mathrm{dc}}} = \frac{2}{\sqrt{3}} mk \approx \frac{2}{\sqrt{3}} \frac{3m\psi_{3r}}{\psi_r} \frac{1}{\sqrt{1 + \left(\frac{L_q i_q}{\psi_r}\right)^2}}. \tag{24}$$

From (23), it can be found that, if $L_q i_q$ is negligible, the $u_{\mathrm{ref}-0}$ amplitude is proportional to m and Ψ_{3r}.

The relationship between m and $u_{\mathrm{ref}-0}$ is shown in Fig. 9. It can be seen that the available maximum ZSV modulation range reduces as m increases according to (20). When $m = 0.866$, the available $u_{\mathrm{ref}-0}$ amplitude is zero, which means that the ZSV reference cannot be modulated. k is decided by the PMSG parameters. In (23), it can be seen that the increase of m will raise the ZSV reference. The trace of $u_{\mathrm{ref}-0}$ reference amplitude will cross over with the available maximum $u_{\mathrm{ref}-0}$ amplitude trace, in which the crossover point means the maximum modulation index on the specific k. In Fig. 10, it can be seen that, in the case $k = 0.2$, 0.1, and 0.05, the corresponding maximum modulation indexes are 0.775, 0.828, and 0.847. It can be concluded that, in order to implement the zero-sequence current suppression, the richer third harmonic component of the rotor flux linkage will cause the lower modulation range. The overmodulation is an inevitable phenomenon since the dc voltage value determines the hexagonal modulation range in $\alpha\beta$ plane and the zero-sequence modulation boundary. Therefore, a larger dc bus voltage could be used to enlarge the modulation range. If the open-winding PMSG operates on the field-weakened region, the modulation index will increase as the motor speed becomes fast. In this case, a higher modulation index is needed to suppress the zero-sequence current which may extend the available modulation range.

VI. Experimental Validation

The experimental system based on the 1-kW open-winding PMSG is developed in the laboratory. In the experimental system, the open-winding PMSG is driven by a 1.5-kW squirrel cage induction machine, and a gearbox with a ratio of 17.08 is used as a mechanical interface. A general converter is used to drive the induction machine. The parameters of an open-winding PMSG are shown in Table III. An adjustable dc power

TABLE III
Open-Winding PMSG Parameters

Parameter	value	Parameter	value
Rated power P_{n}	1kW	Rated speed n	40r/min
Rated phase voltage U_{n}	66.5V	Rated phase current I_{n}	5A
Rated frequency f_{n}	5.33Hz	d-axis inductance L_{d}	77.56mH
Stator R_{s}	1.1Ω	q-axis inductance L_{q}	107.4mH
Pole number n_{p}	8	dc bus voltage	150V

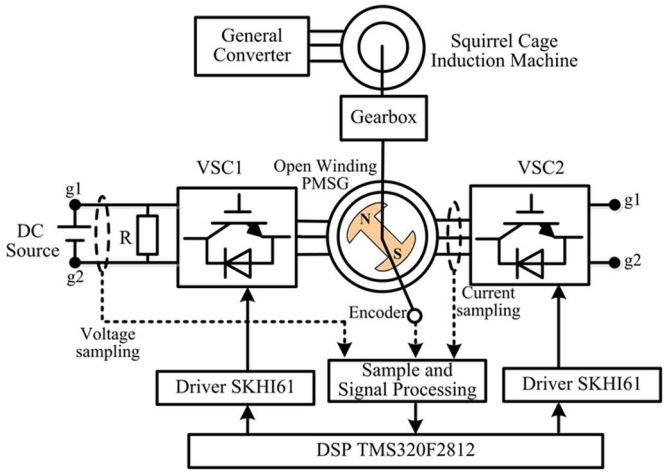

Fig. 11. Open-winding system experimental setup.

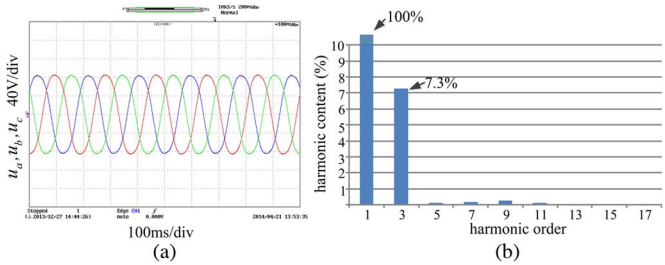

Fig. 12. PMSG back EMF waveform and FFT analysis.

supply is used to establish the dc bus voltage. Both VSCs are built with Semikron SKM75GB124DE IGBTs and connected to the dc source at points g1 and g2. The VSC controller is implemented based on a TMS320F2812, and the driver for IGBT is Semikron SKHI61. The sampling frequency is set as 10 kHz, and the switching frequency of the IGBTs is 5 kHz. The experimental waveform acquisition is obtained by a Yokogawa DL750 scope recorder. In order to focus on the investigation of the zero-sequence current suppression of the open-winding PMSG, a dc power supply is used to replace the grid-side converter. A 20-Ω resistance is paralleled with the dc source to work as the load to consume the energy generated by the open-winding PMSG. The block diagram of the experimental system is shown in Fig. 11.

For the open-winding PMSG, the back EMF waveform with no load and rated speed is shown in Fig. 12. With an FFT analysis, the total harmonic content is 7.38%, while the third harmonic takes up 7.3%. It indicates that the third harmonic content is the main component of back EMF. The influence on

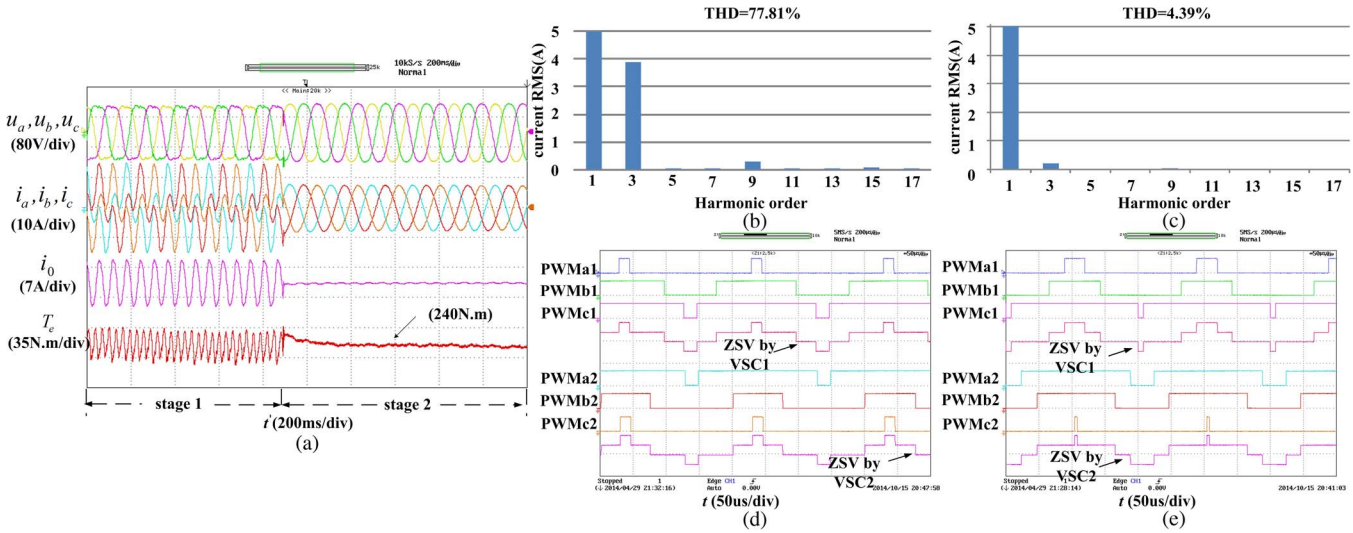

Fig. 13. Waveforms with full-rated load experiment. (a) Waveforms in dynamic response from method 1 and from method 2. (b) FFT analysis on a phase current of stage 1. (c) FFT analysis on a phase current of stage 2. (d) Gating pulses generated by DSP with method 1. (e) Gating pulses generated by DSP with method 2.

zero-sequence current caused by the 9th and 15th components could be neglected.

Fig. 13 shows the waveform comparison with two different control methods. It gives the dynamic response waveforms from method 1 to method 2 at full-rated load as 1-kW active power output. Method 1 is the conventional SVPWM technique shown as stage 1, while method 2 is the proposed method with zero-sequence current elimination controller and ZVR PWM technique shown as stage 2. The experiment is implemented at the rated rotor speed as 40 r/min, while the electrical frequency is rated as 5.33 Hz. The modulation index is 0.6, which is kept in the linear modulation range for ZSV modulation.

From Fig. 13(a), it can be seen that three-phase current takes a rich content of triple harmonic content as controlled with method 1. The amplitude of each phase reaches 13 A, while the zero-sequence's amplitude is 7 A, and the electrical torque fluctuates between 258 and 219 N · m, which means a big vibration for motor working. With the FFT analysis on a phase current in stage 1 shown in Fig. 13(b), it could be found that the third harmonic content is 77.55% compared with the fundamental component. Moreover, in this case, the 9th and 15th harmonics also take content as 5.89% and 1.62%, which could not be neglected. As controlled with method 2, it can be seen that the three-phase current takes a lower triple harmonic content compared with that in method 1. The torque trace presented in Fig. 12 is obtained based on (6). The electrical torque keeps at the value 240 ± 4.3 N · m. The performance is much better than the torque fluctuation from method 1. The amplitude of each phase reaches 7 A, while the zero-sequence current fluctuates with the amplitude as 0.2 A. With the FFT analysis shown in Fig. 13(c), it comes to that the third harmonic content is only 4.25% compared with the fundamental component. Moreover, in this case, the 9th and 15th harmonics take content as 1.93% and 0.46%, which are negligible. The response time takes about 500 ms. Fig. 13(d) shows the gating pulses generated by DSP with method 1. PWMa1–PWMc1 represent the three-phase gating pulses for VSC1, while PWMa2–PWMc2 represent the three-phase gating pulses for VSC2. It also gives the ZSV generated by VSC1 and VSC2. It could be found that the dwell times for (000) and (111) states are nearly the same, and the tiny error is caused by the dead time as 2.3 μs. As a comparison, Fig. 13(e) shows the gating pulses generated by DSP with method 2. The dwell times for (000) and (111) states are redistributed according to the ZSV reference. It can be seen from Fig. 13(b) that, due to neglecting the dead-time effect of the switch device [23], the triple harmonic content is not completely suppressed based on the proposed control scheme.

Fig. 14(a) shows the waveforms of the pole voltages and phase voltage with the proposed ZVR PWM technique within an electrical period. u_{a1N} and u_{a2N}, respectively, represent the pole voltage to negative point in the a-phase, and u_{a1a2} is the phase voltage with the amplitude as $U_{\rm dc}$, 0, $-U_{\rm dc}$. The partially enlarged waveforms of period I and period II are presented in Fig. 14(b) and (c) to give a clear state depiction in the positive and negative half cycles.

Fig. 15 shows the relationship of the current harmonic component and power output at rated rotor speed with methods 1 and 2, respectively. It can be found that, with method 1, the THD content keeps at a high level from 240% to 77% with the power output from 200 W to 1 kW. Obviously, the result applied with method 2 takes a much lower THD content as about 4% for all of the power range. Thus, it comes to a conclusion that method 2 gives a good performance on zero-sequence current suppression. It should be noted that the harmonic range in THD calculation is 0–500 Hz.

The starting performance of the zero-sequence current suppression is presented in Fig. 16. It can be seen that the suppression performance keeps well during the dynamic starting period. The dynamic response with the proposed method based on 50% step changes for the output active power command from 1000 to 500 W was demonstrated in the experiments, with the results shown in Fig. 17. The modulation index changes from 0.6 to 0.607. It can be seen that current trace follows the

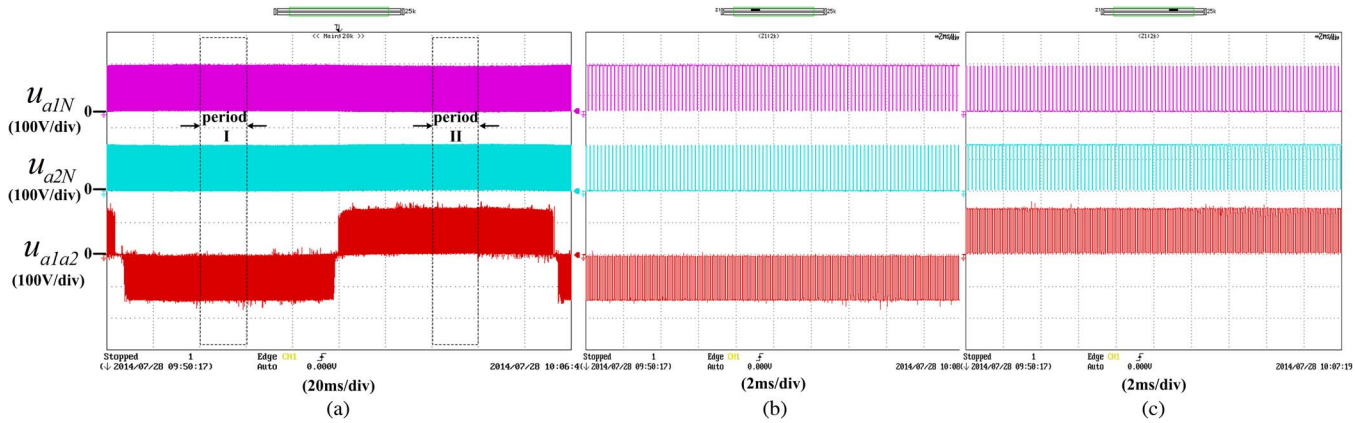

Fig. 14. Waveforms of the pole voltage and phase voltage with method 2. (a) Voltage waveforms within an electrical period. (b) Partially enlarged waveform of period 1. (c) Partially enlarged waveform of period 2.

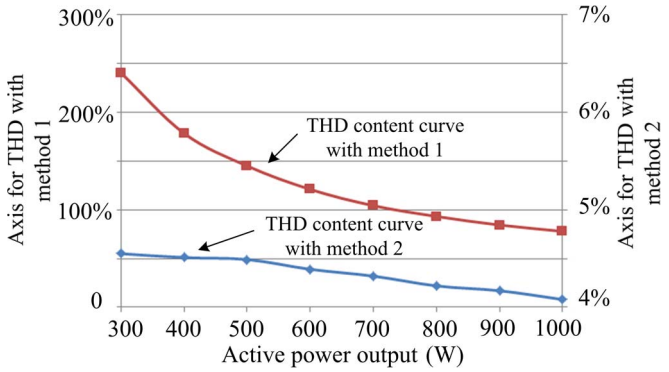

Fig. 15. Comparison on THD contents with different active power outputs between methods 1 and 2.

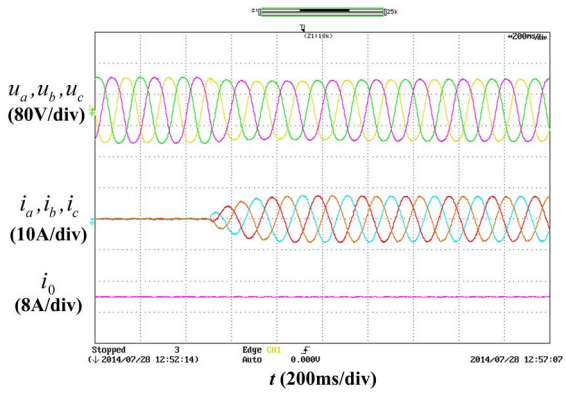

Fig. 16. Starting performance of the open-winding PMSG system with method 2.

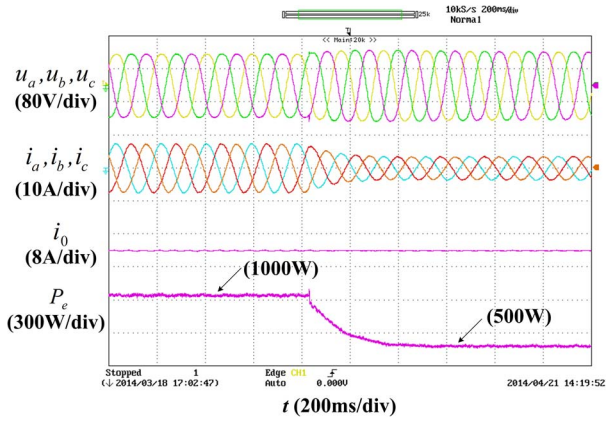

Fig. 17. Dynamic response waveforms from full to half load with method 2.

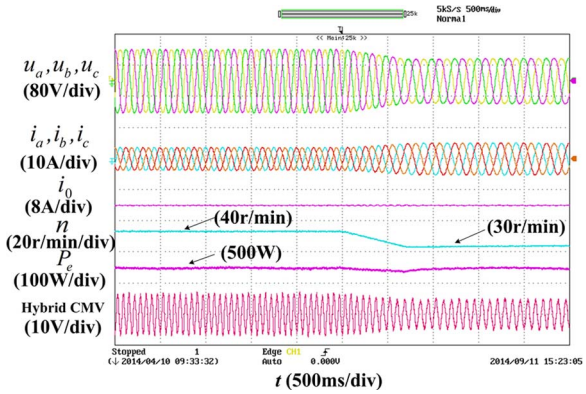

Fig. 18. Dynamic response waveforms from 40 to 30 r/min with method 2.

reference value well. As the power output changes, the zero-sequence content keeps at a low level with the fluctuation within the range of 0 ± 0.3 A. The electrical torque also responses fast and smoothly. The dynamic response time is controlled in 300 ms. The dynamic response with the proposed method based on rotor speed changes from 40 to 30 r/min was also demonstrated in the experiments, with the results shown in Fig. 18. The modulation index changes from 0.607 to 0.442. As the rotor speed changes, the zero-sequence content keeps the fluctuation within the range of 0 ± 0.2 A. The power output is kept as 500 W. In order to present clear waveforms, the CMV waveform is filtered with a cut-off frequency of 500 Hz. It could be found that, with the speed changing from 40 to 30 r/min, the amplitude of ZSV changes from 6.3 to 4.7 V. The dynamic response time is controlled in 300 ms. It proves a good dynamic performance for regular zero-sequence current elimination and ZVR PWM technique.

VII. Conclusion

This paper has proposed a zero current suppression strategy of the open-winding PMSG system based on the ZVR PWM technique. The overall mathematical model of the open-winding PMSG including a zero-sequence circuit has been developed, and a zero-sequence current controller has been designed. The dwell time of the zero vector is redistributed and calculated accurately to obtain the required ZSV reference. The available ZSV modulation range on the different modulation indexes and third back EMF component is also analyzed quantitatively. The experimental results indicate that the proposed zero-sequence current suppression strategy has an excellent steady and dynamic performance for the open-winding PMSG system.

References

[1] Z. Chen, J. M. Guerrero, and F. Blaabjerg, "A review of the state of the art of power electronics for wind turbines," *IEEE Trans. Power Electron.*, vol. 24, no. 8, pp. 1859–1875, Aug. 2009.

[2] M. Liserre, R. Cardenas, M. Molinas, and J. Rodriguez, "Overview of multi-MW wind turbines and wind parks," *IEEE Trans. Ind. Electron.*, vol. 58, no. 4, pp. 1081–1095, Apr. 2011.

[3] K. A. Corzine, M. W. Wielebski, F. Z. Peng, and W. Jin, "Control of cascaded multilevel inverters," *IEEE Trans. Power Electron.*, vol. 19, no. 3, pp. 732–738, May 2004.

[4] B. V. Reddy and V. T. Somasekhar, "A dual inverter fed four level open end winding induction motor drive with a nested rectifier inverter," *IEEE Trans. Ind. Informat.*, vol. 9, no. 2, pp. 938–946, May 2013.

[5] E. Levi, I. N. W. Satiawan, N. Bodo, and M. Jones, "A space vector modulation scheme for multilevel open end winding five phase drives," *IEEE Trans. Energy Convers.*, vol. 27, no. 1, pp. 1–10, Mar. 2012.

[6] B. V. Reddy, V. T. Somasekhar, and Y. Kalyan, "Decoupled space-vector PWM strategies for a four-level asymmetrical open-end winding induction motor drive with waveform symmetries," *IEEE Trans. Ind. Electron.*, vol. 58, no. 11, pp. 5130–5141, Nov. 2011.

[7] V. T. Somasekhar, M. R. Baiju, and K. Gopakumar, "Dual two level inverter scheme for an open-end winding induction motor drive with a single dc power supply and improved dc bus utilization," *Proc. Inst. Elect. Power Appl.*, vol. 151, no. 2, pp. 230–238, Mar. 2004.

[8] M. Narimani and G. Moschopoulos, "Three-phase multimodule VSIs using SHE-PWM to reduce zero-sequence circulating current," *IEEE Trans. Ind. Electron.*, vol. 61, no. 4, pp. 1659–1668, Apr. 2014.

[9] J. moon, C. Kim, J. Park, D. Kang, and J. Kim, "Circulating current control in MMC under the unbalanced voltage," *IEEE Trans. Power Del.*, vol. 28, no. 3, pp. 1952–1959, Jul. 2013.

[10] T. P. Chen, "Circulating zero sequence current control of parallel three phase inverters," *Proc. IEE—Elect. Power Appl.*, vol. 153, no. 2, pp. 282–288, Mar. 2006.

[11] V. T. Somasekhar, K. Gopakumar, E. G. Shivakumar, and A. Petit, "A multilevel voltage space phasor generation for an open end winding induction motor drive using a dual inverter scheme with asymmetrical dc link voltages," *EPE J.*, vol. 12, no. 3, pp. 21–29, May 2009.

[12] J. M. Liu and Z. Q. Zhu, "Improved sensorless control of permanent magnet synchronous machine based on third harmonic back EMF," *IEEE Trans. Ind. Appl.*, vol. 50, no. 3, pp. 1861–1870, May/Jun. 2014.

[13] M. R. Baiju, K. K. Mohaoatra, R. S. Kanchan, and K. Gopakumar, "A dual two-level inverter scheme with common mode voltage elimination for an induction motor drive," *IEEE Trans. Power. Electron.*, vol. 19, no. 3, pp. 794–805, May 2004.

[14] V. T Somasekhar, S. Srinivas, and K. K. Kumar, "Effect of zero-vector placement in a dual-inverter fed open-end winding induction-motor drive with a decoupled space-vector PWM strategy," *IEEE Trans. Ind. Electron.*, vol. 55, no. 6, pp. 2497–2505, Oct. 2008.

[15] V. T Somasekhar, S. Srinivas, and K. K. Kumar, "Effect of zero-vector placement in a dual-inverter fed open-end winding induction motor drive with alternate sub-hexagonal center PWM switching scheme," *IEEE Trans. Power Electron.*, vol. 23, no. 3, pp. 1584–1591, Apr. 2008.

[16] Y. Wang, D. Panda, T. Lipo, and D. Pan, "Open-winding power conversion systems fed by half-controlled-converters," *IEEE Trans. Power Electron.*, vol. 28, no. 5, pp. 2427–2436, May 2013.

[17] J. Hwang and H. Wei, "The current harmonics elimination control strategy for six-leg three-phase permanent magnet synchronous motor drives," *IEEE Trans. Power Electron.*, vol. 29, no. 6, pp. 3032–3040, Jun. 2014.

[18] P. Sandulescu, F. Meinguet, X. Kestelyn, E. Semail, and A. Bruyere, "Control strategies for open-end winding drives operating in the flux-weakening region," *IEEE Trans. Power Electron.*, vol. 29, no. 9, pp. 4829–4842, Sep. 2014.

[19] A. Vidal *et al.*, "Assessment and optimization of the transient response of proportional resonant current controllers for distributed power generation systems," *IEEE Trans. Ind. Electron.*, vol. 60, no. 4, pp. 1367–1383, Apr. 2013.

[20] R. Teodorescu, F. Blaabjerg, M. Liserre, and P. C. Loh, "Proportional-resonant controllers and filters for grid-connected voltage-source converters," *Proc. IEE—Elect. Power Appl.*, vol. 153, no. 5, pp. 750–762, Sep. 2006.

[21] D. G. Holmes and T. P. Lipo, *Pulse Width Modulation for Power Converters: Principles and Practices*. Hoboken, NJ, USA: Wiley-IEEE Press, 2003.

[22] Z. Shu, J. Tang, and J. Lian, "An efficient SVPWM algorithm with low computational overhead for three phase inverters," *IEEE Trans. Power Electron.*, vol. 22, no. 5, pp. 1797–1805, Sep. 2007.

[23] A. Somani, R. K. Gupta, K. K. Mohapatra, and N. Mohan, "On the causes of circulating currents in PWM drives with open end winding ac machines," *IEEE Trans. Ind. Electron.*, vol. 60, no. 9, pp. 3670–3678, Sep. 2013.

Yijie Zhou was born in Xiaogan, China, in 1990. He received the B.Sc. degree from the College of Electrical Engineering, Zhejiang University, Hangzhou, China, in 2011, where he is currently working toward the Ph.D. degree.

His current research interests include motor control with power electronics devices in renewable-energy conversion, particularly the open-winding permanent-magnet synchronous generator systems with integration of multilevel converters.

Heng Nian (M'09) received the B.Eng. and M.Eng. degrees in electrical engineering from Hefei University of Technology, Hefei, China, in 1999 and 2002, respectively, and the Ph.D. degree in electrical engineering from Zhejiang University, Hangzhou, China, in 2005.

From 2005 to 2007, he was a Postdoctoral Researcher with the College of Electrical Engineering, Zhejiang University, where, since 2007, he has been an Associate Professor. His current research interests include optimal design and operation control of wind power generation systems.